Geothermal Reservoir Channel Located by Pressure Transient Analysis: A Numerical Simulation Case Study

Katie McLean[1]* and Sadiq J. Zarrouk[1]

[1]Department of Engineering Science, University of Auckland, Private Bag 92019, Auckland, New Zealand

*** pmcl037@aucklanduni.ac.nz**

Keywords

Pressure transient analysis, well testing, geothermal, numerical simulation, TOUGH2, PyTOUGH, channel boundary.

ABSTRACT

Pressure transient analysis (PTA) of geothermal wells requires numerical models rather than conventional analytical models due to high temperatures and reservoir complexity. For this reason a framework has been recently developed for using numerical simulation for PTA, utilising the TOUGH2 simulator and automated with the PyTOUGH scripting code. The basic radial grid design has the flexibility to include reservoir boundaries by modification of the block volumes and surface areas. In this case study a channel boundary is implemented as two linear impermeable boundaries. The model is then matched to field data from an injection-falloff test in a New Zealand geothermal well. This inverse modelling process utilises software for parameter estimation and uncertainty analysis (PEST). A good match indicates that Well-X lies within a reservoir channel of approximately 130m width. In the process the numerical PTA framework is demonstrated as a viable alternative to analytical PTA. Conventional analytical PTA is included for comparison, utilising the software SAPHIR^{TM}. Both numerical and analytical models require weighting of the intermediate- and late-time field data in order for the model to match during this period. The numerical and analytical model matches appear very similar in the derivative plot and history plot, however the estimated parameters are different. The numerical results are more reliable as they account for the injectate temperature effect.

1. Introduction

Pressure transient analysis (PTA) is problematic for the geothermal industry. Conventional oil and gas methods utilise analytical models which frequently do not fit geothermal field datasets, or they yield unlikely results (McLean and Zarrouk, 2015a). The issue lies fundamentally in the fact that geothermal reservoirs are high temperature with complex structure. Geothermal reservoirs can have temperatures over 300°C, are connected to the wellbore over many hundreds of metres of open hole and contain large networks of fractures. Oil and gas wells are cooler, typically connected over a few tens of metres and usually to a simpler stratified lithology. Due to high temperatures and complexity, geothermal reservoirs violate several fundamental simplifying assumptions which are required for the formulation of analytical models, including the assumptions that the system is isothermal, with uniform and linear fluid properties and horizontal flow (McLean and Zarrouk, 2017).

Therefore complex systems such as geothermal reservoirs require numerical models, which do not require these assumptions to be made. To enable this numerical PTA across the geothermal industry and make it comparable between different wells and well tests, a framework has been established with various guidelines on the model design and other simulation parameters (McLean and Zarrouk, 2017). The basic radial grid design produces a response equivalent to an infinite uniform porous reservoir from analytical PTA theory. The inclusion of reservoir boundaries is achieved by modification of the block volumes and surface areas, and has previously been justified and implemented for a linear impermeable boundary (McLean and Zarrouk, 2017). In this case study a simple modification of the PyTOUGH code includes two linear impermeable boundaries instead of one, thus creating a channel with the well in the centre, which is then applied to field data from an injection-falloff test in Well-X in New Zealand.

2. Background

2.1 Framework for Numerical PTA

A framework has been developed and published as a guide to numerical PTA for geothermal well testing (McLean and Zarrouk, 2017) using the TOUGH2 (Pruess, 1991) reservoir simulator. The objective of the framework is to enable numerical PTA by providing answers to many questions which arise during setup of the model grid and simulation parameters, and also to promote comparability of results. The PyTOUGH scripting code (Croucher, 2011) is used for automation, for example by automating grid generation, model runs and extraction of results. The basic grid design is a radial grid with a central well block, a skin zone in the proximity of the well and a reservoir zone beyond (Figure 1). The well block has special parameters designed to approximate the behaviour of a well during testing, including high porosity, permeability and well compressibility (McLean and Zarrouk, 2017). The process of matching numerical model results to field data is an inverse modelling process which can be achieved for this model using the parameter estimation software PEST, which is model-independent (Doherty, 1994).

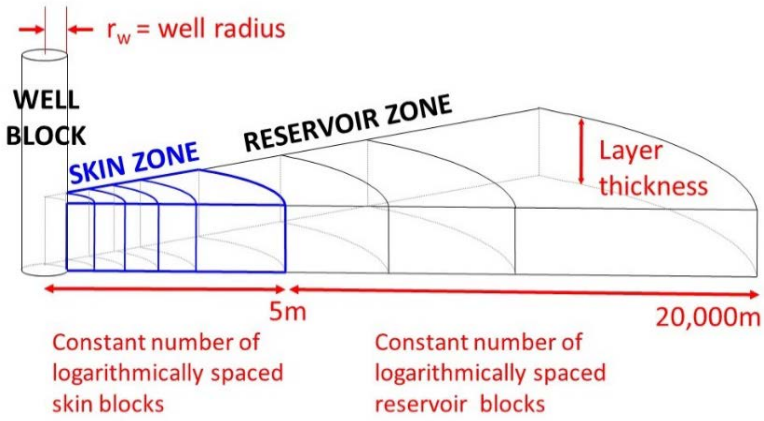

Figure 1: Schematic of radial model design using numerical PTA framework (from McLean and Zarrouk, 2017).

2.2 Linear Impermeable Boundary Model

The basic radial grid of Figure 1 can be modified to represent linear boundaries in the reservoir. Basic geometry can be used to modify the grid block volumes and surface areas as if cut by a linear feature (Figure 2). The calculation only requires specification of a single parameter, the perpendicular distance from the well to the boundary. The calculation of these modified volumes and surface areas and insertion into the TOUGH2 input file is automated within the PyTOUGH script (McLean and Zarrouk, 2017).

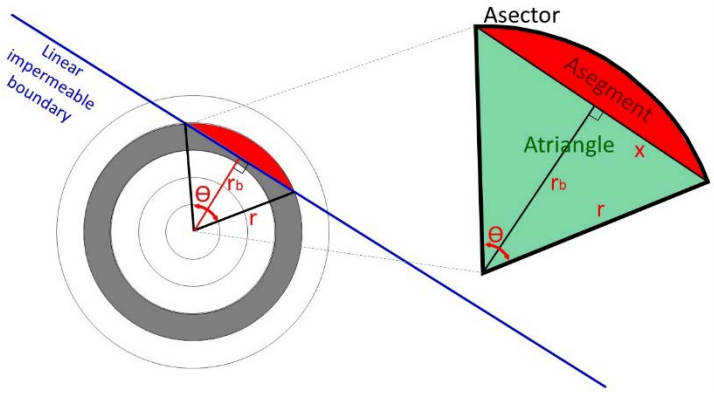

Figure 2: Schematic of modification of radial grid to include a linear impermeable boundary, with definition of geometry elements used in the volume and surface area calculations (from McLean and Zarrouk, 2015b).

3. Field Data

3.1 Well Details and Raw Data

The field data used in this case study comes from Well-X in New Zealand, a large diameter exploration well, which at the time of testing had 13 3/8" production casing and no perforated liner. The open-hole interval is 940m long, with 9 feed zones identified over that length. Injection/fall-off testing was carried out shortly after drilling, with three increasing injection rates (46, 93, 139 m^3/h) followed by a falloff to zero flow (Figure 3a). The downhole pressure-temperature tool is located at the casing shoe rather than within the permeable reservoir due to the possibility of formation collapse in the unlined open-hole section during testing. The reservoir temperature is 172°C and the temperature of the injection water is 27°C at the tool depth immediately prior to the falloff, and is 51°C by the end of the falloff.

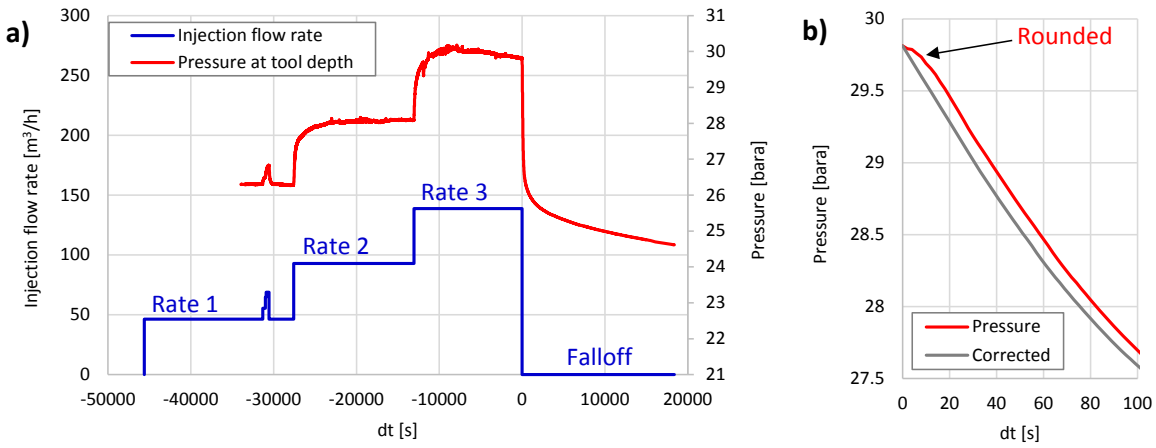

Figure 3: a) Field data: injection flow rate and pressure vs time; b) Close-up of pressure data showing minor rounding at the start of the fall-off, and the corrected data.

In this case the flow rate was only metered during part of injection Rate 1, and not for the remainder of the test. It is therefore not possible to consider analysing the pressure transients as the pressure builds up after the Rate 1-2 flow change or the Rate 2-3 flow change, as the flow data in these periods is based on a single data point and any flow fluctuations are not known. The pressure data is very minorly rounded at the beginning of the fall-off. This is due the impossibility of creating a perfect step-change in flow rate in the real world, however it is easily corrected using the cut-shift-fill method described by McLean and Zarrouk (2015a) (Figure 3b).

3.2 Pressure Derivative and Test Diagnosis

A derivative plot of the fall-off data (Figure 4) is a cornerstone of this analysis and allows for the "diagnosis" of the well test, which is the selection of models which in combination are likely to

fit the field data. The pressure derivative shows many classic features, listed here along with the model chosen to represent them:

- Unit-slope in early-time: wellbore storage model
- Hump during transition: skin model
- Flat derivative in intermediate time: infinite-acting radial flow model (IARF)
- 0.4-unit-slope in late-time: channel boundary model with well in centre

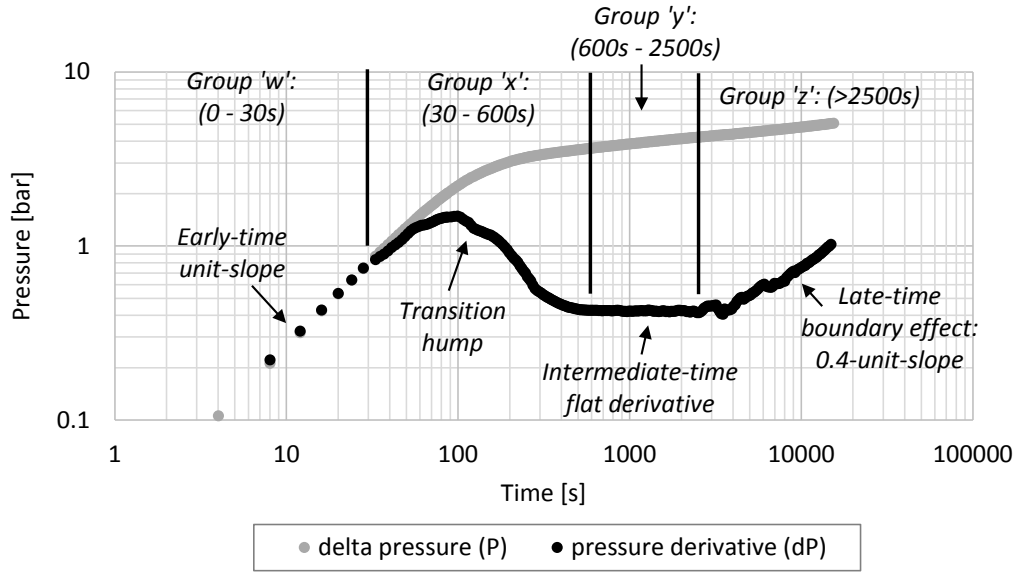

Figure 4: Derivative plot of field data: log-log plot of pressure change (grey) and pressure derivative (black) during the fall-off, showing characteristic features and corresponding observation group definitions.

To aid the inversion process the field observations have been split into four observation groups based on the features of the pressure derivative as listed above (Figure 4):

- Group ‘w’: early-time unit-slope (0 – 30s)
- Group ‘x’: transition (30 – 600s)
- Group ‘y’: intermediate-time flat derivative (600 – 2500s)
- Group ‘z’: late-time boundary (>2500s)

4. Channel Boundary Model

4.1 Implementation in PyTOUGH

The implementation of a channel boundary model in PyTOUGH is achieved via a slight modification of the linear impermeable boundary model script (Section 2.2). The volumes and surface areas to be “removed” by a single linear boundary (Figure 2) are doubled, to represent two boundaries at an equal distance from the well. The channel is characterised by a single

parameter, the distance L from the well centre to both boundaries (Figure 5). The azimuth of the two boundaries shown in Figure 5 is for demonstration only, as it cannot be predicted from a single well PTA.

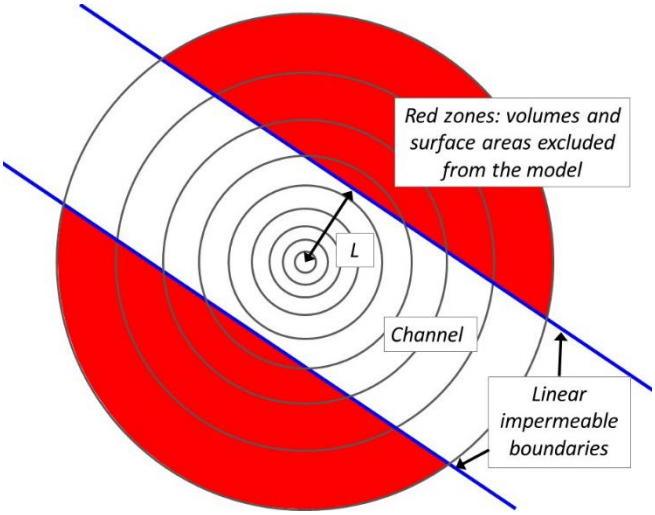

Figure 5: Schematic of radial grid modified by two linear impermeable boundaries with well in centre, characterised by the well-to-boundary distance (*L*).

4.2 Typical Channel Model Response

The derivative plot of Figure 6 shows a typical channel response as the channel narrows from L=500m to L=1m (1000m to 2m total channel width). The response characteristic of a channel is a pressure derivative that rises in an approximately 0.4-unit-slope (Figure 6). For sufficiently long simulations the derivative steepens very slightly in late-time. However, this is unlikely to be observed in field data which are rarely measured for that long. As the channel narrows, the effect of the boundary appears earlier in the data and runs into the transition from wellbore storage. Hence when the channel is very narrow the system never experiences infinite-acting radial flow (IARF), instead transitioning from wellbore storage directly into the boundary response. The pressure responses are curved and appear to have no characteristic features. As the channel narrows (L=1m or L=2m in Figure 6) the pressure response becomes approximately parallel to the derivative response, with 0.4-unit-slope. This resembles the parallel pressure and pressure derivative responses of finite-conductivity or infinite-conductivity fractures, and has an intermediate slope between the two. The finite-conductivity pressure and pressure derivative responses have a 0.25-unit-slope, and the infinite-conductivity responses have a 0.5-unit-slope (Horne, 1995).

It can be seen that the modelled pressure derivative becomes noisy for large values of L e.g. L=1000m in Figure 6. This occurs when the overall pressure change is very small as there is an insufficient number of significant digits available in the TOUGH2 output file to handle such small pressure changes (McLean and Zarrouk, 2015b).

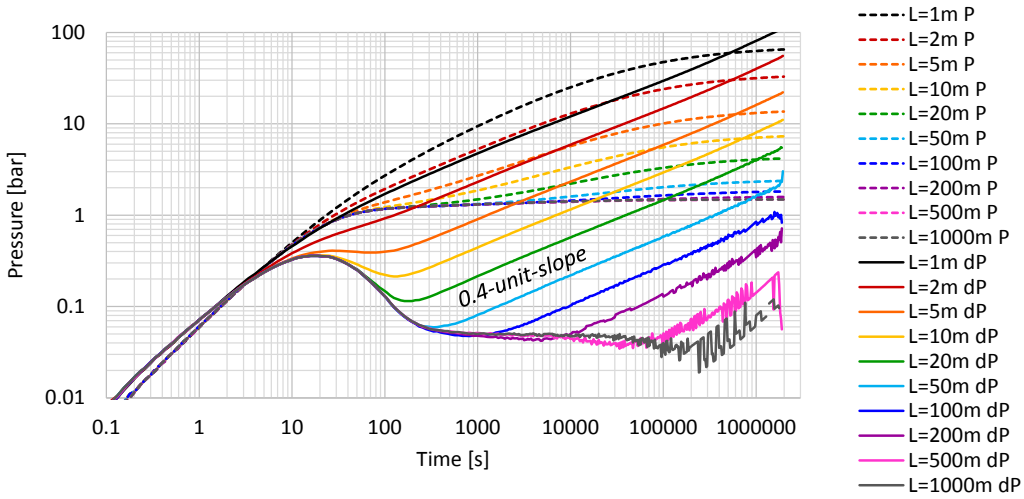

Figure 6: Log-log derivative plot showing typical channel model response: 0.4-unit-slope pressure derivative.

4.3 Setup of Channel Model for Well-X

The numerical model has been set up following the guidelines from the framework (Section 2.1). Only two parameters warrant discussion: the layer thickness chosen to represent the reservoir, and injectate temperature to represent the average temperature of injectate as it goes into the reservoir.

It is known that the model output is sensitive to the layer thickness chosen to represent the reservoir and the guidelines state the entire open-hole length of the well should be used unless it is known that some part can be excluded with certainty (McLean and Zarrouk, 2017). In the case of Well-X the open-hole length is 940m and permeable zones have been observed over that entire length (Section 3.1) and so the model thickness is set at 940m.

The injectate temperature is recommended to be the temperature in the wellbore at the tool depth immediately prior to the fall-off (McLean and Zarrouk, 2015c), which in this case is 27°C. However this number is supposed to represent the average temperature of the injectate at reservoir levels, and the tool during this test is up in the casing shoe, not down in the reservoir. However, this value is still used due to a lack of deeper data. The injectate temperature used will affect the results for skin factor but not permeability (McLean and Zarrouk, 2017).

5. Results and Discussion

5.1 Improving Early-Time Wellbore Storage Match

The well volume V and well compressibility c as estimated by following the guidelines (McLean and Zarrouk, 2017) were 117 m^3 and 1.3e-07 Pa^{-1}. The model response using these fixed parameter values was not a good match to the early-time field data (Figure 7). As these are estimates only, it is legitimate to adjust them slightly to match the early-time data. A good match to the early-time data is obtained in Figure 7 (ignoring any later field data for now) with an adjusted well volume of 100m^3 and well compressibility of 1.1e-07 Pa^{-1} (a decrease of 15% for each).

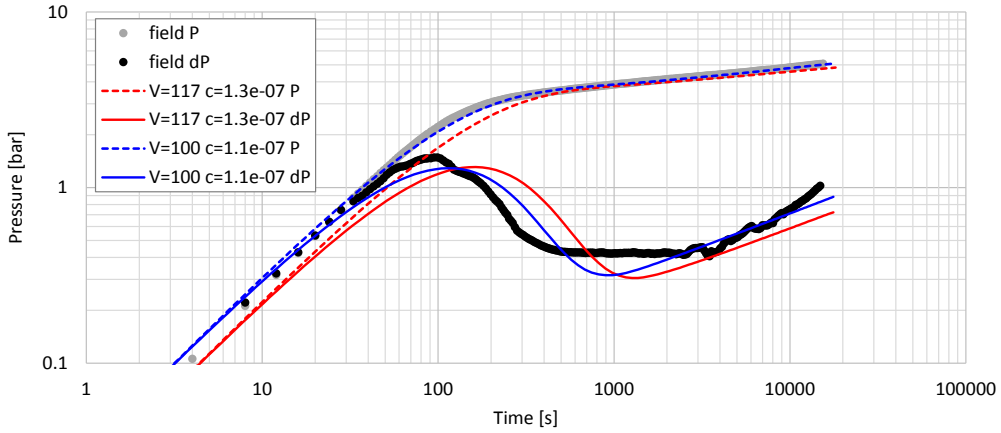

Figure 7: Log-log derivative plot demonstrating effect of adjusting wellbore parameters on model response – entire model response shifts to the left as well volume and compressibility decrease (red to blue).

5.2 Number of Variable Parameters

The fixed parameters well volume V, well compressibility c and injectate temperature T_{inj} are obtained by a process of estimation, as specified in the framework. It logically follows to attempt to obtain estimates for them by allowing these to be variable parameters during the inversion process. The usual four variable parameters are: reservoir permeability k, skin factor s, well to boundary distance L and initial reservoir pressure P_i. As a first attempt, three variable parameters were added: well volume V, well compressibility c and injectate temperature T_{inj} bringing the total to seven variable parameters. The effect of this change is shown in a derivative plot (Figure 8) and the estimated parameters (Table 1).

Confidence limits are narrow for the original four parameter scenario (Table 1). For the seven parameter scenario the estimated values are similar however the confidence limits are so wide these results are useless. Some values in the range are physically impossible, such as injecting water at a negative temperature and a well having a negative volume. Additionally the confidence in the estimated value of skin factor s is significantly decreased due a high correlation between s and T_{inj} which is expected as the injectate temperature effect has the same appearance as skin (McLean and Zarrouk, 2015c).

The derivative plot (Figure 8) shows that the seven parameter scenario sacrifices the early-time match (group ‘w’) for an improved match during the transition period (group ‘x’), a very slight rise in intermediate-time (group ‘y’) and negligible difference in late time (group ‘z’), which is an improved match overall. Fixing both the well volume and compressibility effectively ‘pins’ the response to the early-time unit-slope, which then affects the match at later times. Allowing some wellbore parameters to be variable effectively ‘unpins’ the response in early-time and allows a better overall match to the field data. Despite this improvement in the derivative plot, allowing V, c and T_{inj} to all be variable parameters results in unacceptable levels of uncertainty.

Therefore a further attempt was made by adding only one variable parameter: the well compressibility c for a total of five variable parameters. It is known that well volume and compressibility (V and c) are highly correlated and a decrease in either parameter will shift the

model response to the left on a log-log plot (Figure 7). Therefore the well volume is excluded due to correlation with the compressibility, and also the injectate temperature is excluded due to correlation with the skin factor. The effect of this change is shown in the derivative plot (Figure 8) and estimated parameters (Table 1).

In this case the confidence limits are narrow for all five parameters (Table 1), while retaining the improved shape of the derivative (Figure 8). The very slight rise in the derivative during intermediate time (group 'y') results a decrease in the estimated permeability k from 19.1 mD (four parameters) to 16.1 mD (five parameters). There is also a very minor decrease in skin factor s from -1.7 to -2.1, very minor increase in boundary distance L from 57 to 61m and no change to initial reservoir pressure P_i.

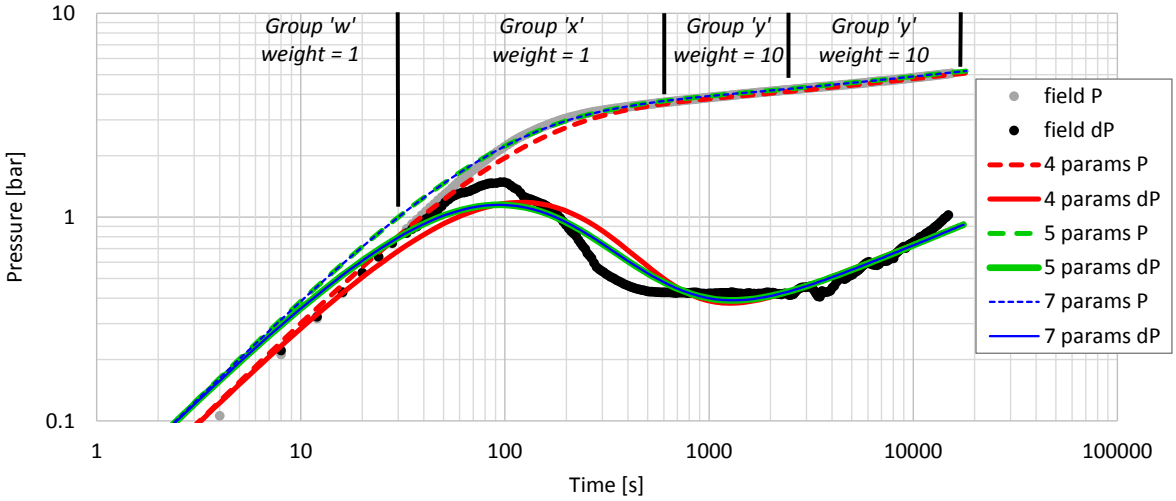

Figure 8: Effect of adding variable parameters to the inversion: original four parameters (red), five parameters (green) and seven parameters (blue).

Table 1: Estimated parameters with 95% confidence limits for four, five and seven variable parameter scenarios.

	Four parameters		*Five parameters*		*Seven parameters*	
Parameter	***Estimated value***	***Confidence limits***	***Estimated value***	***Confidence limits***	***Estimated value***	***Confidence limits***
k [mD]	19.1	18.4 – 19.8	16.1	15.7 – 16.5	16.1	15.6 – 16.6
s	-1.7	-1.8 - -1.6	-2.1	-2.1 - -2.0	-2.1	-3.1 - -1.1
L [m]	57	56 - 58	61	61 - 62	61	60 - 62
P_i [bar]	22.81	22.79 – 22.83	22.81	22.79 – 22.82	22.81	22.79 – 22.83
c [Pa^{-1}]	1.1e-07	(fixed)	8.5e-08	8.3e-08 – 8.8e-08	7.3e-08	-1.6e-08 – 1.6e-07
V [m^3]	100	(fixed)	100	(fixed)	117	-31 - 265
T_{inj} [°C]	27	(fixed)	27	(fixed)	25	-20 – 69

5.3 Improving the Intermediate- and Late-Time Match

A model with five variable parameters (explained in Section 5.2) and no weighting of the observation groupings is the starting point for this inversion process. The resulting estimated parameters are given in Table 2 and derivative plot in Figure 9.

With no weighting of the field observations the model does not reproduce the shape of the field data, specifically it does not reproduce the section of flat derivative, instead cutting through the observations without flattening at the correct level (Figure 9). This model has high permeability (36.6 mD) which sends the derivative below the flat derivative in the field data, and then relies on bringing the boundary closer (42 m) to bend the model response back up towards the field data. In this case infinite-acting radial flow is never achieved and the response goes straight from the transition into the boundary response. In addition to the poor visual match, the 95% confidence limits on the estimated parameters are wide, though not completely unreasonable (Table 2). The value for skin is positive (0.5) which is an unlikely result.

All observation groups should make a comparable contribution to the objective function to ensure that one group does not dominate the inversion process (Doherty, 2010). With no weighting the contributions of groups ‘y’ and ‘z’ (the groups containing the most reservoir information) to the objective function are less than 15% of the total, which is clearly undesirable as the reservoir is of primary interest.

Weighting group ‘y’ and ‘z’ by 10 improves the intermediate- and late-time match (Figure 9). The derivative flattens around the correct level, though the match in the transition period (group ‘x’) is not as good. The contribution of ‘y’ and ‘z’ to the objective function is 56% which is an improvement, however group ‘y’ still contributes four times less than ‘z’. The permeability is lower than the unweighted case (16.1 mD) and the boundary is further away (61m). The skin factor is negative (-2.06) which is far more likely than a positive value as a well drilled with aerated water and no mud has no likely mechanism for the creation of positive skin. The 95% confidence limits are very narrow for all estimated parameters.

One further change is made to the group weighting, to increase the contribution of group ‘y’ to the objective function and improve the match in the section of flat derivative. The weighting of group ‘y’ is increased to 30 and the others left unchanged. The contribution of ‘y’ and ‘z’ to the objective function together becomes 61% and the contribution of ‘y’ is now half that of ‘z’ which is more reasonable. The model match changes very little from the previous case (Figure 9), though the derivative flattens fractionally higher. Thus the estimated permeability is very slightly lower (15.0mD) and also the skin factor is slightly lower (-2.2). All the estimated parameter values are similar to the previous case, and the 95% confidence limits are even narrower.

The results for the second weighted case (weighting w, x, y, z as 1, 1, 30, 10) are the final interpreted results (Table 2): k = 15.0 mD, which means kh = 14100 mD.m for the thickness of 940m, s = -2.2, L = 64m and P_i = 22.83 bara.

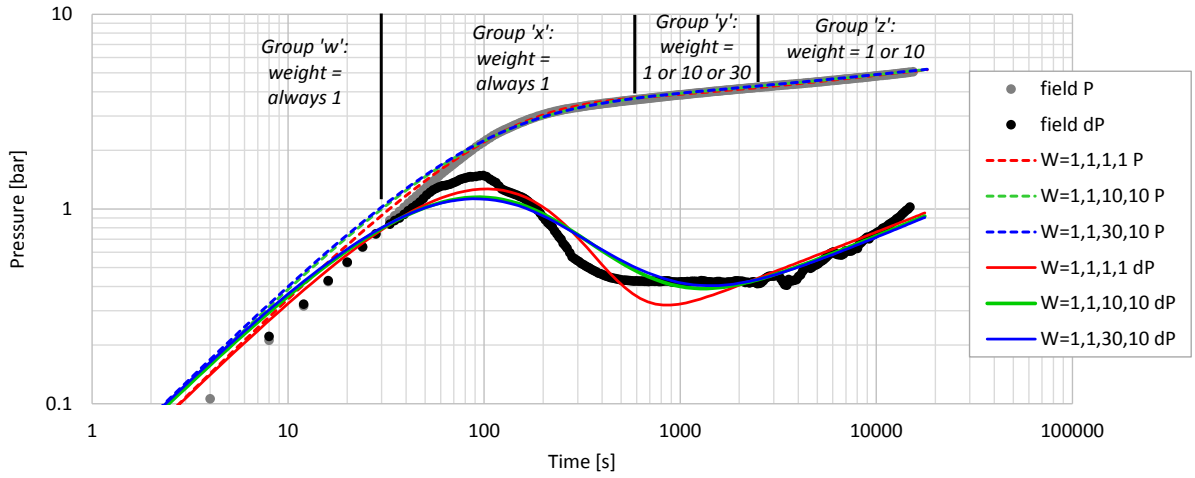

Figure 9: Log-log derivative plot of numerical PTA model responses for three scenarios with different weighting of observation groups.

Table 2: Numerical PTA results: estimated parameters and 95% confidence limits.

Weighting of groups: w, x, y, z		*k [mD]*	*s*	*L [m]*	*P_i [bar a]*	*c [1/Pa]*
1, 1, 1, 1	estimated value	36.6	0.5	42	22.78	9.7e-08
	95% confidence limits	29.2 – 45.9	-0.5 – 1.6	37 - 46	22.75 – 22.82	9.5e-08 – 9.9e-08
1, 1, 10, 10	estimated value	16.1	-2.06	61.4	22.81	8.5e-08
	95% confidence limits	15.7 – 16.5	-2.11 - -2.01	60.5 – 62.2	22.79 – 22.82	8.3e-08 – 8.8e-08
1, 1, 30, 10	estimated value	15.0	-2.20	64.1	22.83	8.2e-08
	95% confidence limits	14.8 – 15.2	-2.23 - -2.18	63.6 – 64.6	22.82 – 22.84	7.9e-08 – 8.5e-08

5.4 Conventional Analytical PTA

Conventional PTA based on analytical models has been carried out on the field data using the software SAPHIR™. This has been done in order to compare the results to those from numerical modelling to see if the results are different and which type of PTA fits the field data best. The "parallel faults" model within SAPHIR™ is the closest equivalent to the numerical channel model. The initial model placement - which is the starting point for the inversion – is generated automatically by the software.

Two inversions are completed, the first an unweighted case and then a weighted case with the same weighting as the best-fit numerical model (Section 5.3). The model fits are shown in a derivative plot in Figure 10 and the corresponding estimated parameters in Table 3.

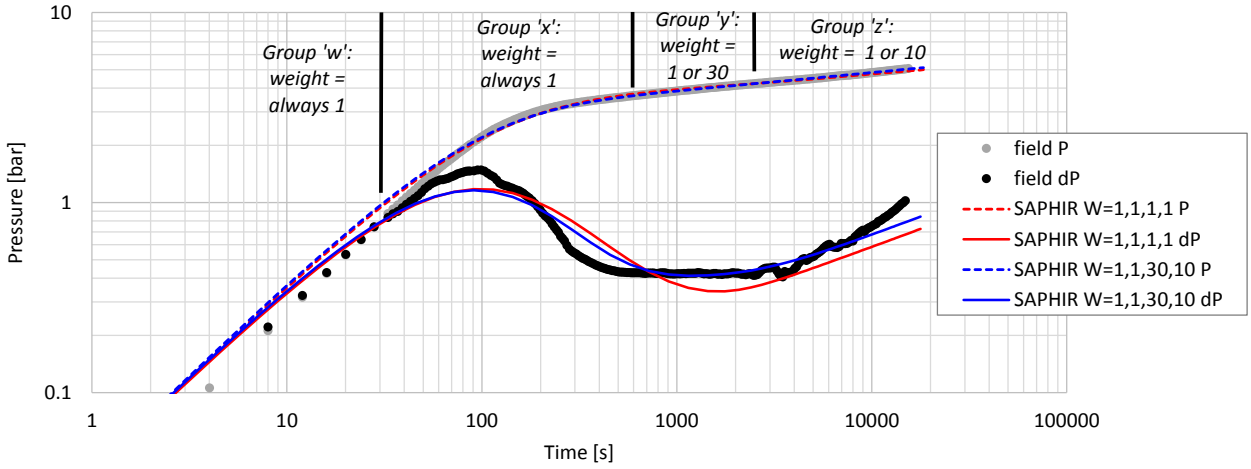

Figure 10: Log-log derivative plot of analytical PTA model responses for two scenarios with different weighting of observation groups.

The initial model match with no weighting is quite close to field data, though the derivative does not flatten at the correct level. Increasing the weighting for late-time data improves the model match for groups ‘y’ and ‘z’ and also slightly for the transition group ‘x’. The analytical software provides less information on the inversion process and hence the contribution of each observation group to the objective function is not known in each case.

One important difference to note between the analytical model and the numerical one is that the analytical parallel faults model estimates the distance to each of the two faults separately. The distances are equal in the unweighted case, and become different for the weighted case when there is more emphasis on the late-time data (Table 3). This raises a fundamental consideration for modelling: models of any complexity can be applied to field data, however the simpler the model the better as long as it can produce a reasonable match. It is a matter of judgement which level of complexity is justified. In this case study the field data has some minor fluctuations in late-time (group ‘z’) which is the group that controls the location of the boundary in the model. To read too much into the exact shape of the field data as it transitions into the boundary response is considered to be an over-analysis in this case. The data is not sufficiently clear in this group to justify this level of detail in the modelling. For this reason no attempt has been made to model the channel boundaries separately for the numerical case (Section 5.3).

Table 3: Analytical PTA results: estimated parameters and 95% confidence limits.

Weighting of groups: w, x, y, z		***k [mD]***	***s***	***L1 [m]***	***L2 [m]***	***P_i [bar a]***
1, 1, 1, 1	estimated value	16.6	0.53	78	78	23.4
	95% confidence limits	16.4 – 16.8	0.46 – 0.60	69 - 88	69 - 88	not given
1, 1, 30, 10	estimated value	19.5	1.31	36.3	87.3	23.1
	95% confidence limits	19.1 – 19.8	1.21 – 1.41	35.1 – 37.5	86 – 88.6	not given

5.5 Isothermal Numerical Simulation

The analytical models are isothermal by necessity, while the numerical model has the advantage of being able to represent the non-isothermal reality of an injection test. Constraining the numerical simulation to the isothermal case is of interest for comparison with the analytical results. This is achieved by specifying the injectate temperature to be the same as the reservoir temperature (172°C). The resulting numerical derivative has a very similar shape to the analytical equivalent (Figure 11) and is indistinguishable from the numerical non-isothermal derivative (not shown). The estimated parameters are given in Table 4 and differ significantly from the non-isothermal results (Table 2) only in terms of the skin factor *s*.

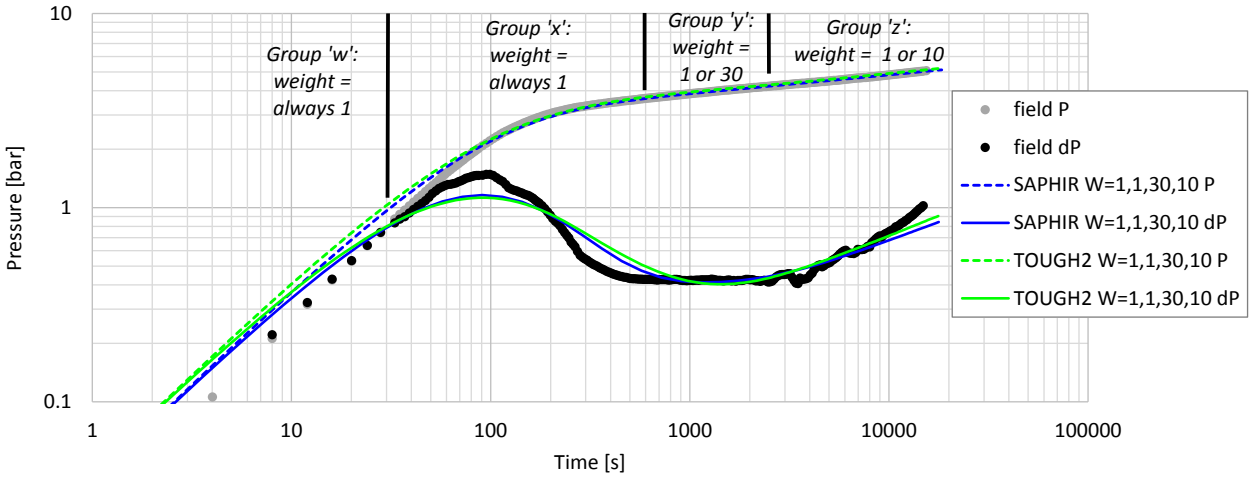

Figure 11: Log-log derivative plot of isothermal numerical and analytical PTA model responses for optimal weighting of observation groups (W=1, 1, 30, 10).

Table 4: Isothermal numerical PTA results: estimated parameters and 95% confidence limits.

Weighting of groups: w, x, y, z		***k [mD]***	***s***	***L [m]***	***P_i [bar a]***	***c [1/Pa]***
1, 1, 30, 10	estimated value	15.3	-0.33	64.7	22.82	8.8e-08
	95% confidence limits	15.1 – 15.5	-0.39 - -0.27	64.2 – 65.2	22.81 – 22.83	8.5e-08 – 9.1e-08

5.6 Local Minimum in the Objective Function

In the numerical unweighted case the model is a poor match to the field data. The derivative would have flattened well below the level of the field data except for the effect of the boundary which pulls the derivative back up again (Figure 9 and 12). The final results were for high permeability, positive skin, and a boundary so close to the well that IARF is never reached. Figure 12 shows that a match with a similar shape and similar estimated parameters can also be obtained with the analytical software (except for skin factor which is higher for the analytical case). This is done by simply choosing a different start point for the inversion in parameter space, rather than using the one automatically generated by SAPHIR^{TM}. These type of results appear to represent a local minimum in the objective function. It is therefore likely that the unweighted numerical match could be improved by simply altering the starting point of the inversion and avoiding this local minima. However this is not considered to be necessary as weighting of some observation groups is required for other reasons (see Section 5.3) and in the process this local minima issue is avoided.

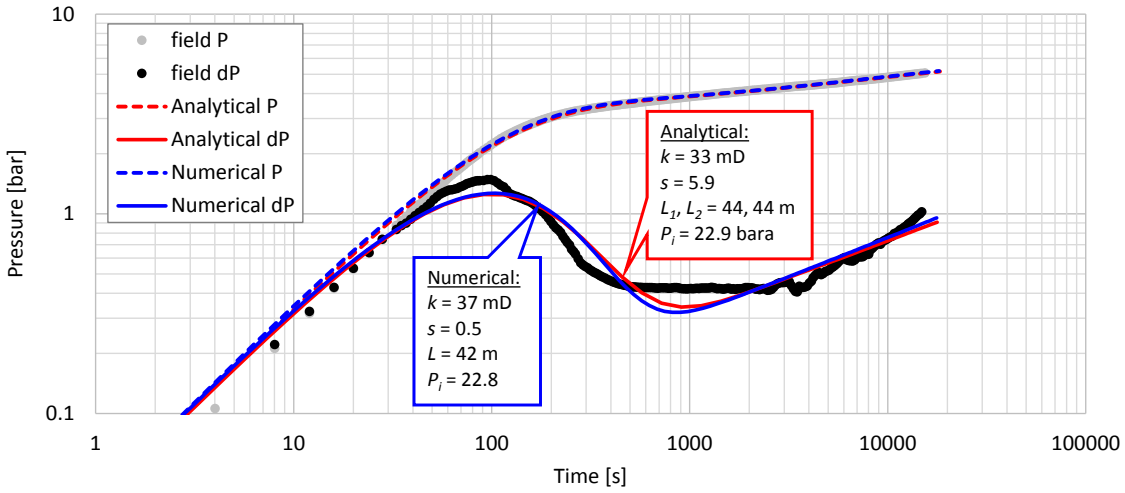

Figure 12: Analytical and numerical model matches in the local minima of the objective function, giving high values for permeability, positive skin and boundaries close to the well.

5.7 Comparison of Numerical and Analytical PTA Results

Good numerical and analytical matches are obtained for a weighting of groups w, x, y, z with weights 1, 1, 30, 10 respectively and the two are directly compared in a derivative plot in Figure 13 and a history plot in Figure 14. The estimated parameters in each case have narrow 95% confidence limits (Tables 2 and 3). The visual quality of the match is very similar and the analytical and numerical model results are indistinguishable from each other and from the field data in the history plot (Figure 14). In the more sensitive derivative plot the pressure derivative reveals very minor differences in the shape of the model results (Figure 13). Both models match the intermediate and late time data very well (groups ‘y’ and ‘z’) partly due to weighting of these groups. Neither model reproduces the shape of the transition data (group ‘x’) very well, in

particular the steepness of the derivative hump. Attempting to reproduce a steeper hump will be the focus of future work as this is a common issue with geothermal well tests. One possible avenue for this will be an implementation of fractional dimension theory (Chang and Yortsos, 1990) into the numerical model.

The results for reservoir permeability k are similar at 15.0 and 19.5 mD (numerical and analytical, respectively). With the reservoir thickness interpreted as 940m this gives a transmissivity kh of 14100 and 18330 mD.m respectively. There is no independent means by which to determine which of the values is the most accurate.

The numerical result for skin is -2.2 (Table 2) which is significantly lower than the analytical value of 1.3 (Table 3). This result is expected as it is known that analytical models overestimate the skin factor in geothermal wells as they do not take account of the effect of injecting cold water into a hot reservoir (McLean and Zarrouk, 2015c). This effect was identified by McLean and Zarrouk (2017) by numerical methods and called the "injectate temperature effect", and also many years previously and independently by Benson and Bodvarsson (1982) by analytical methods and called "fluid skin". The analytical value of s = 1.3 is an overestimate of the skin factor and would mean the well was damaged during drilling, which is unlikely as this well was drilled without mud and aerated water was used to circulate cuttings out of the well. The numerical value of s = -2.2 accounts for the injectate temperature effect and therefore is more likely to be a true reflection of the near-wellbore reservoir condition. The negative skin means the well has been stimulated and a potential mechanism for this is induced fracturing in the near-wellbore region due to in situ stress (e.g. tensile fractures, borehole breakouts and petal-centreline fractures) (Massiot et. al, 2015). The other variable parameters are not independent of s in the inversion process, therefore an incorrect value for s affects the estimates of the other parameters. For this reason all the numerical results are considered to be more reliable, not just s. Numerical simulation of the isothermal case (Section 5.5) produces negligible change to the estimated parameters k, L and P_i and significant change to s, as expected (McLean and Zarrouk, 2017). The skin factor s changes from -2.2 (Table 2) to -0.3 (Table 4) indicating that the overestimation of s to be expected by not accounting for the injectate temperature effect is 1.9. The analytical value of s is 1.3 (Table 3) which is higher than the equivalent isothermal numerical value of -0.3, indicating there may be other factors affecting the determination of s. One possibility may be non-Darcy flow effects (Ramey, 1965) near the well, though unfortunately any flowrate dependence of s cannot be determined as only the falloff data is available for analysis due to a lack of detailed flow data (Section 3.1). The numerical result for the distance from the well to the channel boundaries is L = 64m, which is a channel 128m wide. The analytical distances the boundary are determined independently which is not considered justified as discussed in Section 5.4. However, interestingly, the analytical result is for the two distances L_1 and L_2 to be 36 and 87m which in combination mean a channel 123m wide. So regardless of the detail, both methods predict a channel of practically identical width. Any potential offset of the well from the centre of the channel cannot be determined from this field dataset.

The 95% confidence limits (Tables 2 and 3) are narrow despite high correlations between some parameters, for both the numerical and analytical case. This will be the subject of further investigation to ensure the uncertainty is being estimated reliably.

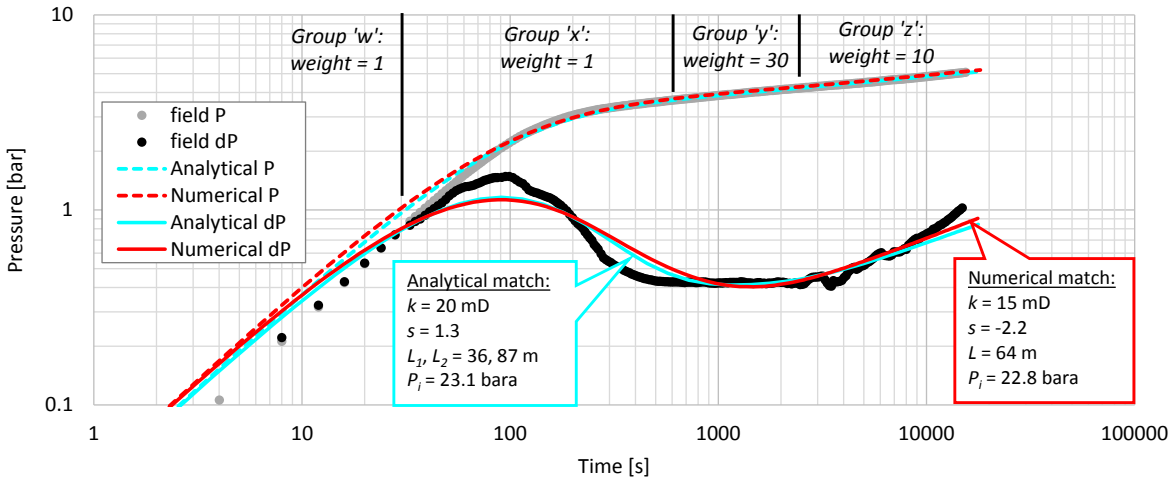

Figure 13: Derivative plot: numerical and analytical best fits (weighting of w, x, y, z = 1, 1, 30, 10).

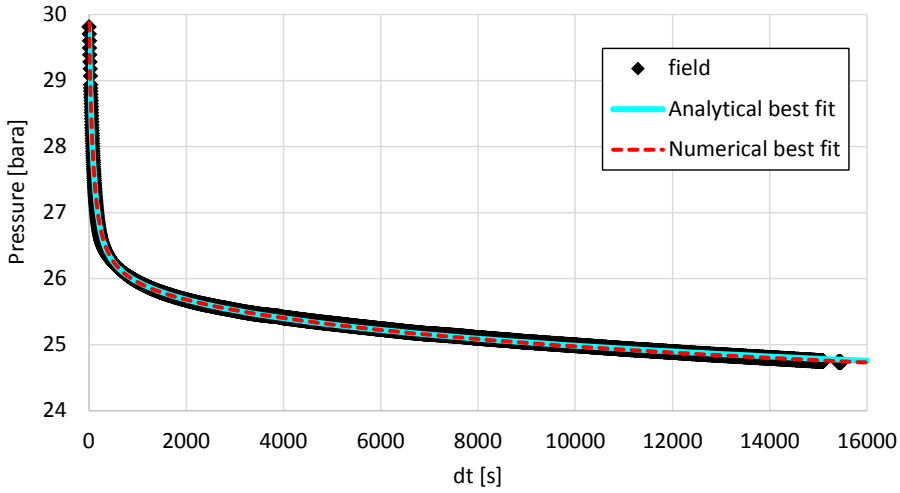

Figure 14: History plot: numerical and analytical best fits (weighting = 10).

6. Conclusions

The linear impermeable boundary variant of the framework for numerical PTA has been successfully adapted to model a channel boundary. This numerical channel boundary model produces a characteristic pressure derivative response of a 0.4-unit-slope rise.

The values for well compressibility and volume as estimated by the guidelines in the numerical PTA framework required minor adjustment in order to match the early-time wellbore storage response. Inclusion of well compressibility *c* as a variable parameter for the inversion was necessary so that the early-time wellbore storage response was not fixed. This removes an unwarranted emphasis on this section of early-time field data and allows a better overall match. Injectate temperature cannot be a variable parameter due to high correlation to the skin factor.

Inversion of the channel model with field data from Well-X produces a good match in both the history plot and derivative plot. As reservoir behaviour is of primary interest in this case, weighting of the intermediate- and late-time data has been applied to improve this match at the expense of the early time match. The resulting match is very good in late time and reasonable in early time, though the steep transition from wellbore storage to reservoir behaviour is not reproduced.

The final numerical PTA results are reservoir permeability k = 15 mD, kh = 14100 mD.m, s = -2.2, L = 64 m and P_i = 22.8 bar with narrow 95% confidence limits. A parallel conventional analytical PTA study of the same field data yields results which have a very similar shape in the history and derivative plot, however with different estimated parameters. The analytical value for skin s = 1.3 is an overestimate due partially to the injectate temperature effect. An isothermal numerical simulation indicates the overestimate of s due to ignoring the injectate temperature effect to be +1.9. As this overestimate will affect all the other estimated parameters from the inversion, the numerical results are considered to be more accurate.

95% confidence limits can be very narrow for both the numerical and analytical case, despite high correlations between some parameters. This will be the subject of further investigation.

Acknowledgement

Mercury Energy Ltd is acknowledged for access to field data. Contact Energy Ltd and the Todd Foundation are acknowledged for financial support. The authors would also like to acknowledge the help of John O'Sullivan at the University of Auckland.

REFERENCES

Benson, S. M. and Bodvarsson, G. S. "Nonisothermal effects during injection and falloff tests." *Technical report, Lawrence Berkeley Lab, CA (USA)* (1982).

Chang, J. and Yortsos, Y. C. "Pressure transient analysis of fractal reservoirs", *SPE Formation Evaluation*, 5(01), (1990) 31--38.

Croucher, A. E. "PyTOUGH: a Python Scripting Library for Automating TOUGH2 simulations" *Proceedings: 33rd New Zealand Geothermal Workshop*, 21-23 November (2011), Auckland, New Zealand.

Doherty, J. "PEST: a unique computer program for model-independent parameter optimisation", *Water Down Under 94: Groundwater/Surface Hydrology Common Interest Papers; Preprints of Papers*, Institution of Engineers, Australia (1994).

Doherty, J. "PEST: Model-Independent Parameter Estimation User Manual", Watermark Numerical Computing (2010).

Horne, R. N. "Modern Well Test Analysis: A Computer-Aided Approach." Petroway Inc (1995).

Massiot, C., McNamara, D. and Lewis, B., "Processing and analysis of high temperature geothermal acoustic borehole image logs in the Taupo Volcanic Zone, New Zealand", *Geothermics*, 53, (2015) 190--201.

McLean, K., and Zarrouk, S. "Pressure transient analysis of geothermal wells: a framework for numerical modelling." *Renewable Energy*, 101, (2017), 737-746.

McLean, K., and Zarrouk, S. "Geothermal well test analysis using the pressure derivative: Some common issues and solutions." *Geothermics*, 55, (2015a), 108-125

McLean, K., and Zarrouk, S. "Linear impermeable boundary in geothermal pressure transient analysis: a reservoir modelling assessment." *Proceedings: 37th New Zealand Geothermal Workshop*, 18-20 November (2015b), Taupo, New Zealand.

McLean, K., and Zarrouk, S. "Impact of cold water injection on geothermal pressure transient analysis: a reservoir modelling assessment." *Proceedings: 37th New Zealand Geothermal Workshop*, 18-20 November (2015c), Taupo, New Zealand.

Pruess, K. "TOUGH2: A general-purpose numerical simulator for multiphase fluid and heat flow." *Lawrence Berkeley Report No. LBL-29400*, Berkeley, California (1991).

Ramey Jr., H.J. "Non-Darcy flow and wellbore storage effects in pressure buildup and drawdown of gas wells." *Journal of Petroleum Technology*, 17(2), (1965), 223-233.